Protein-induced geometric constraints and charge transfer in bacteriochlorophyll-histidine complexes in LH2

Wawrzyniak, P.K.; Alia, A.; Schaap, R.G.; Heemskerk, M.M.; Groot, H.J.M. de; Buda, F.

Protein-induced geometric constraints and charge transfer in bacteriochlorophyll–histidine complexes in LH2†

Piotr K. Wawrzyniak, A. Alia, Roland G. Schaap, Mattijs M. Heemskerk, Huub J. M. de Groot and Francesco Buda*

Bacteriochlorophyll–histidine complexes are ubiquitous in nature and are essential structural motifs supporting the conversion of solar energy into chemically useful compounds in a wide range of photosynthesis processes. A systematic density functional theory study of the NMR chemical shifts for histidine and for bacteriochlorophyll-*a*–histidine complexes in the light-harvesting complex II (LH2) is performed using the BLYP functional in combination with the $6\text{-}311++G(d,p)$ basis set. The computed chemical shift patterns are consistent with available experimental data for positive and neutral$_\tau$ (N$_\tau$ protonated) crystalline histidines. The results for the bacteriochlorophyll-*a*–histidine complexes in LH2 provide evidence that the protein environment is stabilizing the histidine close to the Mg ion, thereby inducing a large charge transfer of ~ 0.5 electronic equivalent. Due to this protein-induced geometric constraint, the Mg-coordinated histidine in LH2 appears to be in a frustrated state very different from the formal neutral$_\pi$ (N$_\pi$ protonated) form. This finding could be important for the understanding of basic functional mechanisms involved in tuning the electronic properties and exciton coupling in LH2.

Introduction

Histidine (His) is one of the 20 naturally occurring amino acids and plays an important role in many biochemical processes. Its imidazole side chain is physically frustrated, between the aromatic and conjugated electronic state, which makes it easy to steer the chemical structure by the biological environment. Histidine can act as a catalyst in the active site of enzymes[1] and as a ligand to metals.[2–7] It can undergo tautomeric changes and is able to form hydrogen bonds, acting both as a proton donor and acceptor, and thus playing the role of a mediator in proton transfer processes in various proteins.[8–9] Four different protonation forms of the imidazole ring are possible, *i.e.* a formally anionic imidazolate form (denoted as negative in this work), two neutral tautomers and a doubly protonated imidazolium form (named positive in this work). The neutral tautomers will be denoted throughout this paper as neutral$_\pi$ and neutral$_\tau$, with N$_\pi$ or N$_\tau$ protonated respectively (see Fig. 1). In the literature N$_\pi$ is sometimes referred to as N$^\delta$ or N$_3$ and N$_\tau$ is indicated as N$^\varepsilon$ or N$_1$. The neutral$_\tau$ histidine is the most frequently found in nature, especially in proteins and smaller compounds.[10–15] The other neutral tautomer is difficult to crystallize and we are aware of only one crystalline sample of glutaric acid–histidine complex where it has been observed.[16] Moreover, it is only occasionally found in proteins

Leiden Institute of Chemistry, Leiden University, P.O. Box 9502, 2300 RA Leiden, The Netherlands.
E-mail: f.buda@chem.leidenuniv.nl; Fax: +31 (0) 715274603;
Tel: +31 (0) 715275723

where it is stabilized by a hydrogen bond and is believed to be reserved for special tasks.[17–19] These two tautomers can be distinguished in a NMR spectrum by their C$_\delta$ chemical shifts.[20] Specifically, values of C$_\delta$ chemical shift above 122 ppm were assigned to the neutral$_\pi$ tautomer, while values below 122 ppm indicate the presence of the neutral$_\tau$. The two nitrogens in the neutral tautomers have substantially different character. The pyrrole-type nitrogen, denoted often as $>$N–H, gives experimentally a NMR signal at 170 ppm and its chemical shift anisotropy in histidine is estimated to be $\delta \approx 4.5$ kHz with $\eta \approx 1$.[13,21,22] On the contrary, the pyridine-type nitrogen, denoted usually as $\geq$N|, gives a NMR signal around 250 ppm, with anisotropy parameters δ and η of about 8.7 kHz and 0.4 respectively.[13,21,22]

Since the histidine activity depends on the nitrogen atoms in the imidazole ring, many biochemical mechanisms may be understood only if the exact histidine protonation states are established. However, according to recent findings, the histidine protonation states reported in Protein Data Bank
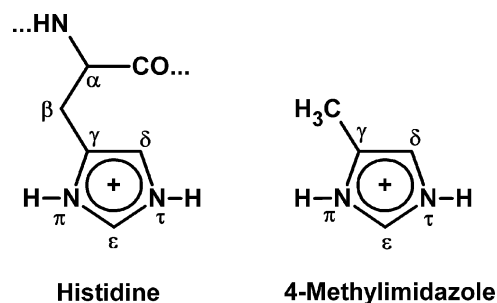

Fig. 1 The labeling of the C and N atoms used throughout the paper for the histidine and 4-methylimidazole models.

structures behave as though they were chosen at random.[23] In principle such information can be obtained from NMR studies.[17,20,24–26] The problem is that even if NMR spectra are available, a precise assignment of the spectral lines to a specific residue is often problematic. Quantum chemical calculations can then provide a complementary tool to assist in resolving the NMR spectra.

The purpose of this study is to demonstrate the viability of this concept for the light-harvesting complex II (LH2) that drives the photosynthesis process in purple bacteria. The structure of LH2 from *Rhodopseudomonas acidophila* (hereafter *Rps. acidophila*) contains a ring of 9 bacteriochlorophyll-*a* (BChl *a*) molecules constituting the so-called B800 system. Additionally another 18 BChl *a* molecules are arranged in pairs (α and β) forming the so-called B850 system.[27] The light absorbed by LH2 is converted into chemical energy by the bacterial reaction center (BRC). While the protonation state of histidines in the BRC has not been clearly assigned so far, a complete assignment of the histidine residues in the LH2 complex of *Rps. acidophila* has been recently obtained by solid-state NMR.[21,28] It was found that the five histidines in the LH2 complex can be classified in two types. The first type, including α-His 37 and β-His 12, has chemical shifts corresponding to neutral$_\tau$ histidines, while the α-His 31, β-His 30 and β-His 41 have been classified as positively charged histidines. However, while the β-His 41 has both nitrogens in the ring protonated, the α-His 31 and β-His 30 are coordinated by the N$_\tau$ to the Mg ion of the bacteriochlorophyll-*a* molecules. Therefore, the residues α-His 31 and β-His 30 are formally neutral$_\pi$ tautomers, which is consistent with the experimental anisotropy parameters for N$_\tau$ indicating a pyridine-like chemical character of this atom.[21,28] Other metal-coordinated histidines maintain their neutral character and show chemical shifts similar to the uncoordinated neutral histidines.[29] Therefore the experimental observation of ^{13}C chemical shifts for the Mg-coordinated histidines identical to those of the positive β-His 41[21,28] is surprising.

In this work we present a complete picture of the NMR chemical shifts for all possible protonation forms of the histidine imidazole ring by using density functional theory (DFT). The neutral$_\pi$ and the negative cases are also included, which, although not much studied in the literature, appear to play an important function in biological systems. Recently it has been argued that the negatively charged histidine may play a role in the electron transfer process in Photosystem II.[30] The results show that DFT is able to predict the pattern of chemical shifts changes upon (de)-protonation for all the histidines in LH2 in good agreement with the experimental data. The findings strongly suggest that the protein environment in LH2 exerts a stress on the histidine coordinated to bacteriochlorophyll resulting in a large charge transfer and a combined structural change. This indicates an anomalous state of physical frustration for those histidines. Finally, the pyridine-like character of the Mg-bound nitrogen in the LH2 complex is addressed, followed by discussion on the effect of hydrogen bonds on the histidine chemical shifts.

The paper is organized as follows: the results and discussion section contains first the calculations for histidine in vacuum in comparison with available experimental data for lyophilized crystalline samples of histidine and a discussion on the accu-

racy of DFT chemical shifts. Next we address the problem of the assignment of the protonation state in non-coordinated and Mg-coordinated histidines in LH2.

Models and methods

All calculations for His and bacteriochlorophyll-*a*–histidine (BChl-His) complexes were performed in vacuum within the DFT framework with the Gaussian 03 package.[31] We applied the BLYP[32–34] exchange–correlation functional, which has already been shown to produce accurate chemical shifts for similar systems.[35] Additionally the B3LYP hybrid functional[33,34,36] was tested (Table S3 in ESI)† and it has a marginal effect on the chemical shifts when compared to BLYP.

Basis set tests were performed for the reference compounds (TMS, NH$_3$) and histidine in all four possible protonation states of its imidazole ring. The discussion is presented in the ESI,† together with the results collected in Tables S1 and S2. Based on these tests, the 6-311++G(d,p) basis set was chosen for the remaining part of the study, except for the geometry optimization of the BChl-His complexes (Fig. 2) where the 6-31++G(d,p) basis set was used.

The initial structure for the BChl-His complex in LH2 was extracted from one of the B850 BChl dimer units of the 2FKW PDB crystallographic structure of *Rps. acidophila*.[27] According to the crystal structure the two BChl molecules in the dimer are slightly asymmetric, but the two histidines coordinated to them appear to be equivalent according to the NMR spectra.[21,28] Therefore we decided to include only one subunit of the dimer, namely β-His 30 and BChl 1601 since we are interested in the characterization of the histidine chemical shifts. To model histidines in a protein environment, a neutral amino acid termination (COOH-NH$_2$) was used to saturate the broken peptide bond. Other protonation states of the amino acid termination that can occur in solution are not of interest in this work. The phytyl tail of the bacteriochlorophyll-*a* was truncated at the ester group and saturated by a hydrogen atom in our model (see Fig. 2). This truncation does not affect the electronic structure of the porphyrin ring.

The geometries were fully optimized and the NMR chemical shieldings were calculated using the gauge-independent atomic orbital (GIAO) method.[37–40] The calculated ^{1}H and ^{13}C chemical shieldings were referred to the tetramethylsilane (TMS) chemical shifts scale, while the computed ^{15}N chemical shieldings were referred to the value of [15]NH$_3$. The experimental chemical shifts referred to ([15]NH$_4$)$_2$SO$_4$ powder were converted to the NH$_3$ scale by adding 20 ppm, as suggested in ref. 41.

The Amsterdam density functional (ADF) program[42–44] was used to calculate the electron charge difference map between the BChl-His complex and its two fragments, histidine and bacteriochlorophyll. In the ADF code the electronic orbitals are written in terms of Slater-type orbitals. The BLYP functional with a TZP (triple-zeta including one set of polarization functions) basis set was used for this calculation.
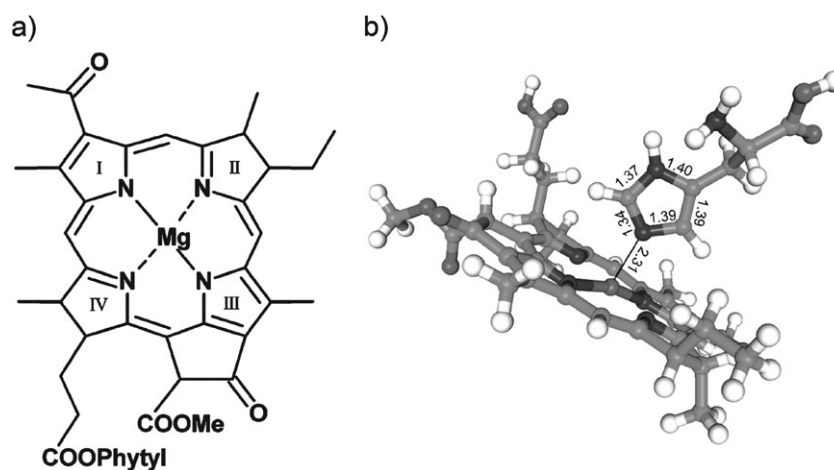
6972 | *Phys. Chem. Chem. Phys.*, 2008, **10**, 6971–6978

This journal is © the Owner Societies 2008

Fig. 2 (a) Schematic representation of the bacteriochlorophyll-*a* structure. (b) DFT-optimized structure of the neutral BChl-*a*–His complex. The phytyl tail was truncated at the ester group and substituted by a hydrogen atom. The bond lengths in the imidazole ring and the Mg-N$_\tau$ distance (Å) are also shown.

Results and discussion

I Chemical shifts calculations of histidine in vacuum

I.1 Geometry. Fig. S1 (see ESI)† shows a comparison of the imidazole ring bond lengths in the DFT-optimized histidine with available crystal structures. Several crystal structures available in the Cambridge Structural Database were analyzed, namely ADAVOQ,[16] ADAVUW,[16] CAMWOD,[45] CAMWUJ,[45] ZOZWAM,[46] as well as the structure determined by Edington *et al.*[47] Interestingly, the ADAVUW structure contains two positive and two neutral$_\pi$ histidines in the unit cell and, according to our knowledge, it is the only evidence of the neutral$_\pi$ tautomer in a simple crystal compound. A very good agreement in the bond lengths is observed for all the available histidine forms, with only a small systematic overestimation of around 2%. This is a typical DFT accuracy for the geometrical parameters, especially taking into account that the specific crystalline environments are neglected. It is worth pointing out that the optimized geometries of the positive and neutral$_\pi$ histidines show an intra-molecular hydrogen bond between N$_\pi$ and the C=O group of the histidine tail.

I.2 Chemical shifts. Table 1 presents a comparison of the calculated histidine chemical shifts with NMR measurements on crystal samples[21,48] available only for histidines with a positive and neutral$_\tau$ imidazole ring[48] (see also Fig. S2 in ESI).† The comparison shows a good agreement for C$_\delta$ and C$_\varepsilon$ (≈ 4 ppm error on average, 3%) and for N$_\tau$ (≈ 12 ppm error on average, 7%). The largest deviations are observed for C$_\gamma$ (16 ppm, 13%) and N$_\pi$ (60 ppm, 25%). Unfortunately, for the neutral$_\pi$ tautomer, only selected chemical shifts within various protein environments have been reported.[20] However, this tautomer has been already observed in a simple compound[16] and could be used in the future as a generic model for chemical shifts of neutral$_\pi$ histidine. Interestingly, DFT predicts that the three ^{13}C signals in neutral$_\pi$ histidine should appear very close to each other, contrary to the other three forms, as can be seen in Table 1. Moreover, the condition

mentioned in the introduction to distinguish between the two neutral tautomers[20] is satisfied by the computed C$_\delta$ chemical shifts.

A direct comparison for the doubly deprotonated histidine is also not possible as it has never been clearly observed experimentally. According to the results in Table 1 the most peculiar feature of the negative form is the remarkably large C$_\varepsilon$ chemical shift value of 154 ppm, which is about 20 ppm downfield compared to the other three cases. This prediction supports the suggestion that a doubly deprotonated histidine may be present in the Photosystem II.[30]

Table 1 contains also the chemical shifts computed for two neutral tautomers of the 4-methylimidazole. These chemical shifts are very similar to those of neutral histidines, except for N$_\pi$ in the neutral$_\pi$ tautomer where a difference of 7 ppm is observed. When adding a water molecule forming an inter-molecular hydrogen bond to 4-MeIm at the π position, the N$_\pi$ chemical shift has almost the same value as in neutral$_\pi$ histidine. This result shows that the inter-molecular and the intra-molecular H-bond have the same effect on the N$_\pi$ chemical shift. It can be also noticed that the chemical shifts of C$_\varepsilon$ are almost equal in the two neutral tautomers due to the symmetry of the ring.

Apart from comparing absolute values, it is also useful to compare the chemical shift changes upon protonation or deprotonation of the imidazole ring. In this way systematic DFT errors are partially cancelled and it is easier to identify trends that may help in the assignment of histidine protonation states. Fig. 3a presents the experimental, denoted as 'Exp. Crystal', and DFT chemical shift difference between positive and neutral$_\tau$ histidines defined as $\Delta\delta = \delta_{form1} - \delta_{form2}$. The pattern in $\Delta\delta$ is correctly reproduced by the calculation. The largest deviations from experiment are found for the N$_\tau$ (7.7 ppm) and N$_\pi$ (23 ppm) nitrogens.

I.3 Source of error for chemical shifts. The comparison between theoretical and experimental chemical shifts exhibits an overall good agreement for the carbon atoms. The largest deviation is observed for C$_\gamma$, possibly due to the large effect of

Table 1 Calculated histidine and 4-methylimidazole (4-MeIm) chemical shifts [ppm] for different protonation states in comparison with available experimental data for crystal histidine. The experimental values for ^{15}N are converted to NH$_3$ as a reference compound (see section on computational details). 'x' denotes an inter-molecular hydrogen bond with a water molecule at the pyrrole nitrogen

	Histidine (exp.)[a]		Histidine (DFT BLYP/6-311++G(d,p))					4-MeIm (DFT BLYP/6-311++G(d,p))		
	Positive	Neutral$_\tau$	Positive	Neutral$_\tau$	Neutral$_{\tau}\cdots$x	Neutral$_\pi$	Negative	Neutral$_\tau$	Neutral$_\pi$	Neutral$_{\pi}\cdots$x
C$_\gamma$	128.0	137.0	144.3	148.5	147.7	131.6	137.7	147.3	129.8	130.7
C$_\delta$	119.3	113.5	122.6	117.9	118.0	134.5	133.4	113.9	133.6	133.4
C$_\varepsilon$	136.4	138.6	132.9	136.0	137.1	137.3	154.0	136.3	136.8	137.0
N$_\pi$	175	242	212	302	301	190	293	306	183	192
N$_\tau$	172	167	188	175	186	303	295	174	304	302
H$_\delta$			7.2	6.9	6.9	7.0	7.0	6.7	6.9	6.8
H$_\varepsilon$			8.0	7.4	7.5	7.3	7.4	7.3	7.3	7.4

^{a} ^{13}C chemical shifts from ref. 21, ^{15}N chemical shifts from ref. 48.

the environment on this particular carbon, related to the tail orientation. Indeed C$_\gamma$ is known to be sensitive to the protein environment and for that reason is not used for discriminating between the two neutral tautomers.[20]

Although the pyrrole or pyridine character of the nitrogens in the different protonation states is correctly reproduced by the calculation, significant differences with the experimental values are observed for ^{15}N chemical shifts. Due to the high polarizability of the nitrogen atom, hydrogen bonding and other intermolecular interactions strongly affect the ^{15}N chemical shieldings.[22,49–52] By neglecting those effects, the standard deviation between experimental and DFT ^{15}N chemical shifts may be as large as 30 ppm,[53] which is 18% of the protonated ^{15}N chemical shift value. Moreover, even if those intermolecular interactions are included, an error of 17 ppm (10%) is still observed.[53] These previous findings are in line with the errors observed in the present calculations. A considerable effort is under way in finding efficient ways of including the environmental effects in the chemical shift calculations through embedding schemes at various level of accuracy.[54–56] An explicit inclusion of the crystal environment is outside the scope of the present work. In conclusion, some care should be taken when comparing DFT absolute chemical shifts with experimental data, especially for nitrogen atoms. The comparison of relative chemical shifts is more reliable since the error is partially cancelled out, as may be seen in Fig. 3.

II   Protonation state of histidines in the light-harvesting Complex II

II.1.   Non-coordinated histidines (α-His 37, β-His 12, β-His 41). Experimentally resolved NMR chemical shifts for histidines in LH2 are shown in Table 2. The proposed assignment was based on the experimental values for crystal samples of histidine.[21,28] It was also suggested, based on the nitrogen chemical shifts, that some of the histidines in LH2 are involved in hydrogen bond interactions.[21,28] The chemical shift difference $\Delta\delta$ between the positively charged β-His 41 and the neutral α-His 37 is shown in Fig. 3a (Exp. LH2) together with the computed $\Delta\delta$ between positive and neutral$_\tau$ histidine in vacuum (DFT). The experimental pattern is correctly reproduced: The $\Delta\delta$ for C$_\gamma$ and C$_\varepsilon$ is predicted to be −4.2 ppm ($\Delta\delta^{exp}$ = −8.6 ppm) and −3.1 ppm ($\Delta\delta^{exp}$ = −3.0 ppm), respectively, while for C$_\delta$ it is +4.7 ppm ($\Delta\delta^{exp}$ = +4.8 ppm). Finally, a large chemical shift difference of 72 ppm is observed experimentally for N$_\pi$, while no change occurs for N$_\tau$. The theoretical results also show a large difference of 90 ppm for N$_\pi$, while N$_\tau$ is predicted to shift by 13 ppm. The ^{1}H signals are also reproduced very well, both in absolute and relative values (see Tables 1 and 2).

Fig. 3b presents the experimental chemical shifts difference $\Delta\delta$ between α-His 37 and β-His 12 (Table 2) compared with the computed $\Delta\delta$ between neutral$_\tau$ and neutral$_\tau$ including a hydrogen bonded water at the N$_\tau$ site (Table 1). This comparison reveals that the presence of a hydrogen bond affects mainly the N$_\tau$ chemical shift and confirms the experimental suggestion that β-His 12 is involved in a hydrogen bond.[21,28]
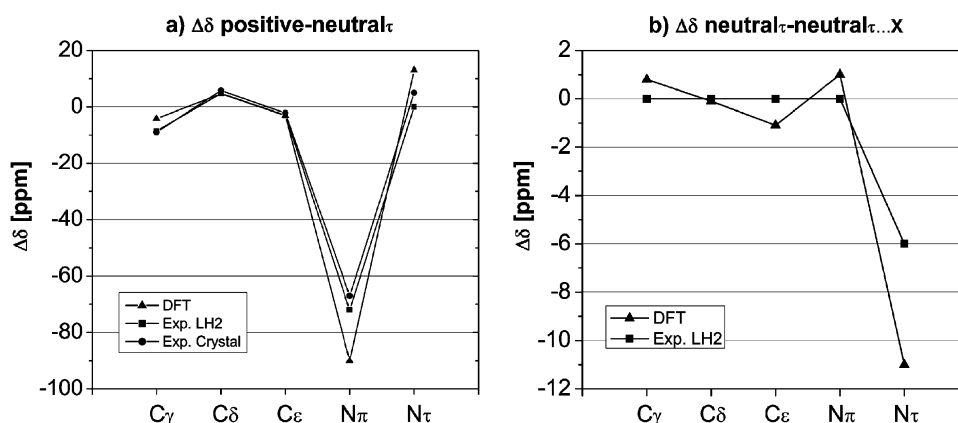
Fig. 3 (a) Chemical shift difference $\Delta\delta = \delta_{\text{positive}} - \delta_{\text{neutral}_\tau}$ [ppm] based on DFT calculations, histidine crystal samples[21,48] and β-His 41, α-His 37 in LH2.[21,28] (b) Chemical shift difference $\Delta\delta$ [ppm] between neutral$_\tau$ tautomer and neutral$_\tau$ with H-bond on the N_τ based on DFT calculations and α-His 37, β-His 12 in LH2.[21,28]

II.2 Mg-coordinated histidines (α-His 31, β-His 30). The DFT results for various BChl-a–His complex models are collected in Table 2. It has been suggested that these Mg-coordinated histidines may be involved in hydrogen bonding on the N_π side with the C13^1-keto carbonyl of the adjacent bacteriochlorophyll-a molecule.[21,28] Therefore we studied complexes **2**, **4** and **5**, which include an inter-molecular hydrogen bond between N_π and a water molecule. The structure of the BChl-a-His complexes **1** and **2** was fully optimized, while the complexes **3** and **4** were kept fixed according to the crystallographic data.[27] The complex **5** was partially optimized in the presence of some geometrical constraints, as explained below.

By comparing the chemical shifts for the complexes with and without the hydrogen bond, we see that the main effect is a change of 8 ppm in the chemical shift of the pyrrole-type nitrogen. Since this type of nitrogen gives a NMR resonance at 170 ppm, the observed chemical shift value of 178 ppm for N_π in Mg-coordinated histidine can be indeed attributed to the presence of a hydrogen bond. However, a careful analysis of the X-ray structure in the vicinity of the β-His 30 leads to the conclusion that the hydrogen bond partner is the alanine β-Ala 26 and not the keto carbonyl of the adjacent BChl-a molecule suggested earlier.[21,28] Thus, the Ala 26 C=O forms two hydrogen bonds with His 30, one with the backbone NH and one with the side chain N_π. A similar situation occurs for the α-His 31 and α-Ala 27.

The computed chemical shifts for the imidazole protons H$_\delta$ and H$_\epsilon$ in the BChl-a –His complexes (Table 2) clearly show a ring current effect of about 4 ppm when compared with the values for the non-coordinated histidines (Table 1), which is in very good agreement with the experiment.

The ^{13}C experimental data for the Mg-coordinated histidines are the same as those of the positively charged histidine, suggesting that a charge transfer is taking place from the histidine to the bacteriochlorophyll.[21,28] The DFT ^{13}C chemical shifts are in much better agreement with the experimental values when the X-ray structure is considered without performing a geometry optimization (Table 2, complexes **2** and **4**). This result suggests that the constraints due to the protein environment have a significant effect on the electronic

structure of the BChl-His complex. The comparison between the crystallographic data and the optimized geometry shows that (i) the N_τ-Mg distance increases from 2.12 Å to 2.31 Å in the DFT-optimized structure, (ii) the dihedral angle φ defined by N4, Mg, N_τ, and C$_\epsilon$, which represents the rotation of histidine around the Mg–N_τ axis, increases from 32° to 48°, and (iii) the BChl ring becomes more flat. These changes in the geometry corresponds to a change in the total charge of the histidine from 0.2 for the complex **2** to 0.5 for the complex **4**, clarifying why the formally neutral$_\pi$ Mg-coordinated histidine in LH2 behaves as a positive histidine according to the ^{13}C NMR data.

According to the X-ray data the imidazole ring of β-His 30 shows bond lengths typical for doubly protonated histidines. However, the RMSD on the bond lengths in the LH2 X-ray data is 0.03 Å, which is about the bond length difference between positive and neutral$_\pi$ histidines. Therefore we additionally performed a constrained geometry optimization of the BChl-His complex in which only the imidazole ring was relaxed keeping fixed the N_τ–Mg distance and the dihedral angle φ defined above. It was found that: (i) the charge transfer is essentially the same as obtained using the non-optimized crystal structure; (ii) a RMSD of 4.5 ppm for the ^{13}C chemical shifts resulting from this partially optimized structure is the same as for the crystal structure (see Table 2, complex **5**); (iii) the bond lengths in the imidazole ring are now systematically shorter by 0.01–0.02 Å with respect to the fully optimized structure (see also Fig. S3 in ESI).† It can be concluded that the charge transfer depends crucially on the relative distance and orientation of the BChl-His complex. This charge transfer can be clearly visualized by computing the charge density difference between the BChl-a–His complex and the two fragments, His and BChl, separately (Fig. 4). The DFT results strongly suggest that the protein environment is forcing the histidine to stay close to the BChl, thereby inducing a combined structural change and a large charge transfer.

Although the ^{13}C data show the character of a positively charged histidine, the Mg-coordinated N_τ still maintains its pyridine character.[21] This is also confirmed by the calculated anisotropy parameters for N_τ in the complex **5**: The computed δ and η are 8.9 kHz and 0.5, respectively, vs. 8.4 kHz and 0.4

Table 2 Calculated and experimental chemical shifts for histidines in the LH2 complex. In the schematic representation of the model, the histidine tail and the remaining part of the BChl-a molecule were omitted for clarity. The indicated charge of histidine is the formal charge. NH···X denotes a hydrogen bond. The structure of the complexes **1** and **2** was fully optimized, the complexes **3** and **4** correspond to the X-ray structure of LH2,[27] while the complex **5** was partially optimized (see section II.2 for details)

	Experiment LH2[a]				DFT BLYP/6-311++G(d,p)				
	β-His 12	α-His 37	β-His 41	α-His 31, β-His 30	**1**	**2**	**3**	**4**	**5**
C_γ	133.7	133.7	125.1	125.1	133.6	134.1	129.5	130.0	128.8
C_δ	113.5	113.5	118.3	118.3	129.7	128.6	124.5	123.7	125.2
C_ϵ	136.5	136.5	133.5	133.5	135.6	136.5	132.2	131.4	134.3
N_π	250	250	178	178	188	196	175	183	196
N_τ	176	170	170	225	277	277	281	278	273
H_δ	6.2	6.2	6.5	2.6	3.0	2.9	4.6	4.4	3.8
H_ϵ	7.4	7.4	7.9	4.2	3.1	3.2	3.3	3.6	4.7

[a] From ref. 21 and 28.

estimated from NMR measurements[21] and agree well with the values expected for pyridine-type nitrogen. These results emphasize the state of frustration, especially for the N_τ.

This finding of a protein-induced charge transfer in the BChl-His complex may have important effects on the absorption spectra and excitation energy transfer processes observed in LH2. Not only the excitation site energies and transition dipole moments of the BChl-His complex, but also the long-range electrostatic interactions with the protein environment may change significantly. Preliminary time-dependent DFT calculations performed on the BChl-His model show a significant effect mainly on the Q_x absorption band when compared to the isolated BChl. This result appears to be in line with absorption spectroscopy studies of BChl a in solvents.[57] Of course a proper study of these effects needs an explicit inclusion of the environment.[58] In a recent DFT study, Neugebauer[59] has addressed the issue of the environmental effects on the excitation energies and photophysical properties of LH2 complexes. However, in that study the histidine has been modeled by a frozen density embedding approach, which may be inappropriate if indeed charge transfer is taking place. Further investigations on these issues are needed but are outside the scope of the present work.

Conclusions

We have presented a comprehensive analysis of the chemical shifts for different protonation states of the histidine imidazole ring using DFT at the BLYP/6-311++G(d,p) level. The comparison with experimental data for crystal samples shows that trends can be predicted with good accuracy and that the largest errors are observed for pyridine type nitrogen atoms that may be strongly affected by the specific environment.

The DFT chemical shifts support the recently proposed assignment of the histidine protonation state in LH2 and confirm that all the histidines except α-His 37 participate in a hydrogen bond. Moreover, the results put forward the idea that the protein environment in LH2 exerts a stress on the Mg-coordinated histidines that induces a considerable electron charge transfer to the bacteriochlorophylls. This explains why these histidines behave as though positively charged and not as neutral$_\pi$. This observed charge transfer may have far-reaching consequences on the absorption properties and photophysics of the BChl macrocycle in the LH2 dimeric B850 complex and we hope that this work will stimulate further investigations in this direction. The understanding of these basic functional mechanisms will guide the design of future artificial photosynthesis devices.
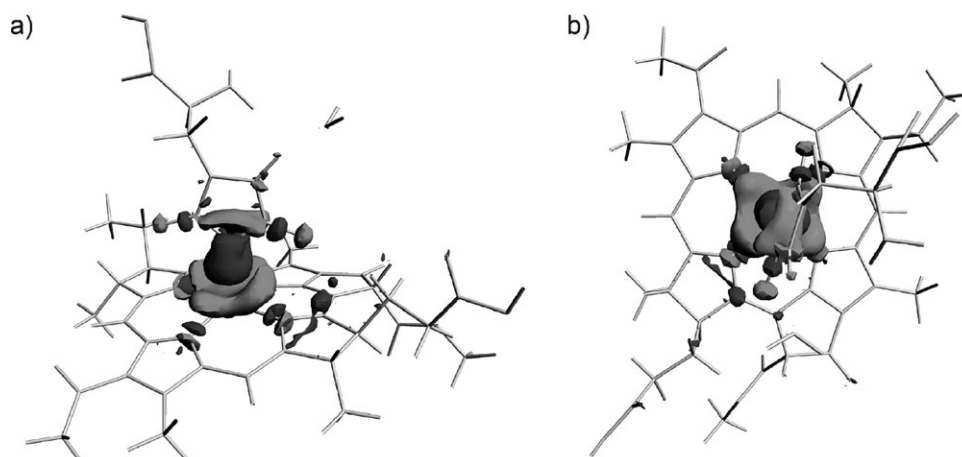
Acknowledgements

Fig. 4 Change in the electronic density upon BChl-His complex formation, calculated for the partially optimized structure (see text for details). The isosurface value is 0.0012 e/Å^3. The lighter colour corresponds to an increase of the density in the complex, as compared to the separated BChl and His fragments, while the darker colour denotes a decrease in the electronic density. (a) Side view and (b) top view.

from the University of Wrocław for providing access to their computer resources. Jörg Matysik is very much thanked for fruitful discussions. We also acknowledge one of the referees for suggesting the constrained optimization of the BChl-His complex, which helped to clarify the important geometric factors influencing the charge transfer.

References

1 S. A. Krupenko, A. P. Vlasov and C. Wagner, *J. Biol. Chem.*, 2001, **276**, 24030.
2 L. Banci, M. Benedetto, I. Bertini, R. Del Conte, M. Piccioli and M. S. Viezzoli, *Biochemistry*, 1998, **37**, 11780.
3 C. N. Fuhrmann, B. A. Kelch, N. Ota and D. A. Agard, *J. Mol. Biol.*, 2004, **338**, 999.
4 L. E. Dardenne, A. S. Werneck, M. D. Neto and P. M. Bisch, *Proteins-Structure Function and Genetics*, 2003, **52**, 236.
5 B. Vallone, K. Nienhaus, A. Matthes, M. Brunori and G. U. Nienhaus, *Proc. Natl. Acad. Sci. USA*, 2004, **101**, 17351.
6 A. V. Giri, S. Anishetty and P. Gautam, *BMC Bioinf.*, 2004, **5**, 127.
7 A. S. Lipton, R. W. Heck and P. D. Ellis, *J. Am. Chem. Soc.*, 2004, **126**, 4735.
8 Z. D. Zhang, E. A. Komives, S. Sugio, S. C. Blacklow, N. Narayana, N. H. Xuong, A. M. Stock, G. A. Petsko and D. Ringe, *Biochemistry*, 1999, **38**, 4389.
9 A. G. Harrison, *Mass Spectrom. Rev.*, 1997, **16**, 201.
10 W. F. Reynolds, I. R. Peat, M. H. Freedman and J. R. Lyerla, *J. Am. Chem. Soc.*, 1973, **95**, 328.
11 T. H. Huang, W. W. Bachovchin, R. G. Griffin and C. M. Dobson, *Biochemistry*, 1984, **23**, 5933.
12 A. Ramamoorthy, C. H. Wu and S. J. Opella, *J. Am. Chem. Soc.*, 1997, **119**, 10479.
13 Y. F. Wei, A. C. de Dios and A. E. McDermott, *J. Am. Chem. Soc.*, 1999, **121**, 10389.
14 T. Gajda, B. Henry and J. J. Delpuech, *J. Chem. Soc. Perkin Trans*, 1994, **2**, 157.
15 N. Shimba, H. Takahashi, M. Sakakura, I. Fujii and I. Shimada, *J. Am. Chem. Soc.*, 1998, **120**, 10988.
16 N. T. Saraswathi and M. Vijayan, *Acta Cryst.*, 2001, **B57**, 842.
17 R. M. Day, C. J. Thalhauser, J. L. Sudmeier, M. P. Vincent, E. V. Torchilin, D. G. Sanford, C. W. Bachovchin and W. W. Bachovchin, *Protein Sci.*, 2003, **12**, 794.
18 W. W. Bachovchin and J. D. Roberts, *J. Am. Chem. Soc.*, 1978, **100**, 8041.
19 W. W. Bachovchin, *Proc. Natl. Acad. Sci. USA*, 1985, **82**, 7948.
20 J. L. Sudmeier, E. M. Bradshaw, K. E. Coffman Haddad, R. M. Day, C. J. Thalhauser, P. A. Bullock and W. W. Bachovchin, *J. Am. Chem. Soc.*, 2003, **125**, 8430.
21 Alia, J. Matysik, C. Soede-Huijbregts, M. Baldus, J. Raap, J. Lugtenburg, P. Gast, H. J. van Gorkom, A. J. Hoff and H. J. M. de Groot, *J. Am. Chem. Soc.*, 2001, **123**, 4803.
22 M. S. Solum, K. L. Altmann, M. Strohmeier, D. A. Berges, Y. L. Zhang, J. C. Facelli, R. J. Pugmire and D. M. Grant, *J. Am. Chem. Soc.*, 1997, **119**, 9804.
23 G. F. Signorini, R. Chelli, P. Procacci and V. Schettino, *J. Phys. Chem. B*, 2004, **108**, 12252.
24 H. Günther, *NMR-Spektroskopie, 361*, Georg Thieme Verlag, Stuttgart, 1992.
25 D. Canet, *NMR-Konzepte und Methoden, 184*, Springer-Verlag, Berlin, 1994.
26 J. Evans, *Biomol. NMR Spectr., 71*, Oxford University Press, Oxford, 1995.
27 V. Cherezov, J. Clogston, M. Z. Papiz and M. Caffrey, *J. Mol. Biol.*, 2006, **357**, 1605.
28 Alia, J. Matysik, I. de Boer, P. Gast, H. J. van Gorkom and H. J. M. de Groot, *J. Biol. NMR*, 2004, **28**, 157.
29 S. S. Kidambi, D. K. Lee and A. Ramamoorthy, *Inorg. Chem.*, 2003, **42**, 3142–3151.
30 A. Diller, E. Roy, P. Gast, H. J. van Gorkom, H. J. M. de Groot, C. Glaubitz, G. Jeschke, J. Matysik and A. Alia, *Proc. Natl. Acad. Sci.*, 2007, **104**, 12767.
31 M. J. Frisch, G. W. Trucks, H. B. Schlegel, G. E. Scuseria, M. A. Robb, J. R. Cheeseman, J. A. Montgomery, Jr., T. Vreven, K. N. Kudin, J. C. Burant, J. M. Millam, S. S. Iyengar, J. Tomasi, V. Barone, B. Mennucci, M. Cossi, G. Scalmani, N. Rega, G. A. Petersson, H. Nakatsuji, M. Hada, M. Ehara, K. Toyota, R. Fukuda, J. Hasegawa, M. Ishida, T. Nakajima, Y. Honda, O. Kitao, H. Nakai, M. Klene, X. Li, J. E. Knox, H. P. Hratchian, J. B. Cross, V. Bakken, C. Adamo, J. Jaramillo, R. Gomperts, R. E. Stratmann, O. Yazyev, A. J. Austin, R. Cammi, C. Pomelli, J. Ochterski, P. Y. Ayala, K. Morokuma, G. A. Voth, P. Salvador, J. J. Dannenberg, V. G. Zakrzewski, S. Dapprich, A. D. Daniels, M. C. Strain, O. Farkas, D. K. Malick, A. D. Rabuck, K. Raghavachari, J. B. Foresman, J. V. Ortiz, Q. Cui, A. G. Baboul, S. Clifford, J. Cioslowski, B. B. Stefanov, G. Liu, A. Liashenko, P. Piskorz, I. Komaromi, R. L. Martin, D. J. Fox, T. Keith, M. A. Al-Laham, C. Y. Peng, A. Nanayakkara, M. Challacombe, P. M. W. Gill, B. G. Johnson, W. Chen, M. W. Wong, C. Gonzalez and J. A. Pople, *GAUSSIAN 03 (Revision C.02)*, Gaussian, Inc., Wallingford, CT, 2004.
32 A. D. Becke, *Phys. Rev. A*, 1988, **38**, 3098.
33 C. T. Lee, W. T. Yang and R. G. Parr, *Phys. Rev. B*, 1988, **37**, 785.
34 B. Miehlich, A. Savin, H. Stoll and H. Preuss, *Chem. Phys. Lett.*, 1989, **157**, 200.

35 J. C. Facelli, *J. Phys. Chem. B*, 1998, **102**, 2111.
36 A. D. Becke, *J. Chem. Phys.*, 1993, **98**, 5648.
37 R. McWeeny, *Phys. Rev.*, 1962, **126**, 1028.
38 R. Ditchfie, *Mol. Phys.*, 1974, **27**, 789.
39 K. Wolinski and A. J. Sadlej, *Mol. Phys.*, 1980, **41**, 1419.
40 K. Wolinski, J. F. Hinton and P. Pulay, *J. Am. Chem. Soc.*, 1990, **112**, 8251.
41 *Principal Components of Chemical Tensors: A Compilation*, ed. T. Michael Duncan, The Farragut Press, Madison, WI, 2nd edn, 1997, ISBN: 0-917903-14-5.
42 G. te Velde, F. M. Bickelhaupt, S. J. A. van Gisbergen, C. Fonseca Guerra, E. J. Baerends, J. G. Snijders and T. Ziegler, *J. Comput. Chem.*, 2001, **22**, 931.
43 C. Fonseca Guerra, J. G. Snijders, G. te Velde and E. J. Baerends, *Theor. Chem. Acc.*, 1998, **99**, 391.
44 ADF2007.01 SCM, *Theoretical Chemistry*, Vrije Universiteit, Amsterdam, The Netherlands, http://www.scm.com.
45 N. T. Saraswathi and M. Vijayan, *Acta Cryst.*, 2002, **B58**, 734.
46 V. H. Vilchiz, R. E. Norman and S. C. Chang, *Acta Cryst.*, 1996, **C52**, 696.
47 P. Edington and M. M. Harding, *Acta Cryst.*, 1974, **B30**, 204.
48 M. Munowitz, W. W. Bachovchin, J. Herzfeld, C. M. Dobson and R. G. Griffin, *J. Am. Chem. Soc.*, 1982, **104**, 1192.
49 K. L. Anderson-Altmann, C. G. Phung, S. Mavromoustakos, Z. W. Zheng, J. C. Facelli, C. D. Poulter and D. M. Grant, *J. Phys. Chem.*, 1995, **99**, 10454.
50 J. C. Facelli, R. J. Pugmire and D. M. Grant, *J. Am. Chem. Soc.*, 1996, **118**, 5488.
51 J. Z. Hu, J. C. Facelli, D. W. Alderman, R. J. Pugmire and D. M. Grant, *J. Am. Chem. Soc.*, 1998, **120**, 9863.
52 M. B. Ferraro, V. Repetto and J. C. Facelli, *Solid State NMR*, 1998, **10**, 185.
53 J. C. Facelli, *J. Biomolec. Struct. & Dynamics*, 1998, **3**, 619.
54 C. R. Jacob and L. Visscher, *J. Chem. Phys.*, 2006, **125**, 194104.
55 J. Schmidt, A. Hoffmann, H. W. Spiess and D. Sebastiani, *J. Phys. Chem. B*, 2006, **110**, 23204.
56 S. Komin, C. Gossens, I. Tavernelli, U. Rothlisberger and D. Sebastiani, *J. Phys. Chem. B*, 2007, **111**, 5225.
57 L. Limantara, S. Sakamoto, Y. Koyama and H. Nagae, *Photochem. Photobiol.*, 1997, **65**, 330.
58 F. Müh, M. El-Amine Madjet, J. Adolphs, A. Abdurahman, B. Rabenstein, H. Ishikita, E. Knapp and T. Renger, *Proc. Natl. Acad. Sci. USA*, 2007, **104**, 16862.
59 J. Neugebauer, *J. Phys. Chem. B*, 2008, **112**, 2207.